IFT-UAM/CSIC-24-66

How to rule out $(g-2)_\mu$ in $U(1)_{L_\mu - L_\tau}$ with White Dwarf Cooling

Patrick Foldenauer [1,*] and Jaime Hoefken Zink [2,3,†]

[1] *Instituto de Física Teórica, Universidad Autónoma de Madrid, 28049 Madrid, Spain*
[2] *Dipartimento di Fisica e Astronomia, Università di Bologna, via Irnerio 46, 40126 Bologna, Italy*
[3] *INFN, Sezione di Bologna, viale Berti Pichat 6/2, 40127 Bologna, Italy*

(Dated: May 2, 2024)

In recent years, the gauge group $U(1)_{L_\mu - L_\tau}$ has received a lot of attention since it can, in principle, account for the observed excess in the anomalous muon magnetic moment $(g-2)_\mu$, as well as the Hubble tension. Due to unavoidable, loop-induced kinetic mixing with the SM photon and Z, the $U(1)_{L_\mu - L_\tau}$ gauge boson A' can contribute to stellar cooling via decays into neutrinos. In this work, we perform for the first time an *ab initio* computation of the neutrino emissivities of white dwarf stars due to plasmon decay in a model of gauged $U(1)_{L_\mu - L_\tau}$. Our central finding is that an observation of the early-stage white dwarf neutrino luminosity at the 30% level could exclude (or partially exclude) the remaining allowed parameter space for explaining $(g-2)_\mu$. In this work, we present the relevant white dwarf sensitivities over the entire A' mass range. In particular, we have performed a rigorous computation of the luminosities in the resonant regime, where the A' mass is comparable to the white dwarf plasma frequencies.

arXiv:2405.00094v1 [hep-ph] 30 Apr 2024

I. INTRODUCTION

Our current best theory of physics at the smallest scales is in terms of the Standard Model (SM) of particle physics. Despite its enormous success, the SM leaves some of the most pressing questions of elementary particle physics unanswered. Most prominently, both an explanation of the small masses of neutrinos, and the existence of dark matter (DM) require physics beyond the SM (BSM). A particularly simple and well-motivated extension of the SM is given by a new gauged $U(1)_{L_\mu - L_\tau}$ symmetry [1–4]. This not only allows to accommodate neutrino masses [5–8] and DM [9–15], but can also help to explain the muon $(g-2)_\mu$ anomaly [16–19], the Hubble tension [20–22] and the $b \to s\,\mu\mu$ anomaly [23–27].

In the absence of elementary kinetic mixing, the associated gauge boson only couples to second- and third-generation leptons. This makes $U(1)_{L_\mu - L_\tau}$ models generically hard to test at earth-based laboratory experiments, since couplings to conventional matter, i.e. quarks and electrons, are only induced at the one-loop level via kinetic mixing with the photon. However, its gauge couplings to mu- and tau-flavoured neutrinos render neutrino interactions an excellent way of searching for $U(1)_{L_\mu - L_\tau}$ bosons [28]. In particular, for $U(1)_{L_\mu - L_\tau}$ bosons lighter than the dimuon threshold almost all leading constraints are due to tests of neutrino physics, like neutrino trident production [23], neutrino oscillation measurements at Borexino [29, 30], the number of effective neutrino degrees of freedom $N_{\rm eff}$ during big bang nucleosynthesis (BBN) [20, 31, 32], or neutrino cooling of supernovae (SN) [33, 34].

A theoretically very clean astrophysical environment to study neutrino physics is provided for by early-stage, hot White Dwarfs (WD). Their behaviour is well understood and the various existing equations of state (EoS) for modelling WDs reproduce identical results for the same conditions [35–39]. In the initial stage of the life of WDs, their evolution is governed by neutrino cooling via plasmon decay into neutrinos exiting the WD core [40, 41]. The cooling through plasmon decay could in principle be enhanced by strong magnetic fields or through the addition of new fields that could connect SM neutrinos with the electron-positron loop [42–53]. An additional $U(1)_{L_\mu - L_\tau}$ boson, for example, can in principle enhance the plasmon decay into neutrinos via its kinetic mixing with the photon and thus modify the evolution of WDs. This will ultimately lead to a modification of the WD luminosities compared to the SM prediction. Previously, the resulting constraint on the $U(1)_{L_\mu - L_\tau}$ parameter

* patrick.foldenauer@csic.es
† jaime.hoefkenzink2@unibo.it

space has been estimated [54] via an effective field theory (EFT) analysis of modified plasmon decays in WDs [55]. In this paper, however, we will perform an *ab initio* calculation of the modified WD luminosities due to a $U(1)_{L_\mu - L_\tau}$ gauge boson correctly taking into account transverse, axial and longitudinal emissivities as well as the fully gauge-invariant kinetic mixing.

The remainder of this article is organised as follows. In Section II, we introduce the theoretical framework of the minimal $U(1)_{L_\mu - L_\tau}$ model studied in this paper. In Section III, we present the computation of the neutrino luminosities responsible for WD cooling within $U(1)_{L_\mu - L_\tau}$. Finally, we present our results in Section IV before presenting our conclusions in Section V.

II. THE $U(1)_{L_\mu - L_\tau}$ MODEL

The Lagrangian of the SM exposes some accidental global symmetries like baryon number, $U(1)_B$, and the lepton family numbers, $U(1)_{L_i}$ with $i = e, \mu, \tau$. Remarkably, the combinations $U(1)_{B-L}$ and $U(1)_{L_i - L_j}$ with $i, j = e, \mu, \tau$ can be promoted to anomaly-free gauge symmetries with only the SM field content.[1] Among these anomaly-free groups $U(1)_{L_\mu - L_\tau}$ is of special phenomenological interest as it allows for the explanation of several experimental anomalies. For example, it can accommodate the observed excess in the anomalous magnetic moment of the muon $(g-2)_\mu$, as well as the tension arising from determining the Hubble constant H_0 from early-time cosmology via the cosmic microwave background (CMB) [56] contrasted with the value obtained from local measurements via standard candles like type-Ia supernovae and cepheid variable stars [57].[2]

The relevant parts of the Lagrangian of an extra $U(1)_{L_\mu - L_\tau}$ symmetry can be compactly written in matrix form as

$$\begin{aligned}\mathcal{L} \supset &- \frac{1}{4}\,(B_{\alpha\beta}, W^3_{\alpha\beta}, X_{\alpha\beta}) \begin{pmatrix} 1 & 0 & \epsilon_B \\ 0 & 1 & \epsilon_W \\ \epsilon_B & \epsilon_W & 1 \end{pmatrix} \begin{pmatrix} B^{\alpha\beta} \\ W^{3\alpha\beta} \\ X^{\alpha\beta} \end{pmatrix} \\ &+ \frac{1}{2}\,(B_\alpha, W^3_\alpha, X_\alpha)\, \frac{v^2}{4} \begin{pmatrix} g'^2 & g'\,g & 0 \\ g'\,g & g^2 & 0 \\ 0 & 0 & \frac{4\,M_X^2}{v^2} \end{pmatrix} \begin{pmatrix} B^\alpha \\ W^{3\alpha} \\ X^\alpha \end{pmatrix} \\ &- (g'\,j^\alpha_Y,\ g\,j^\alpha_3,\ g_{\mu\tau}\,j^\alpha_{\mu\tau}) \begin{pmatrix} B_\alpha \\ W^3_\alpha \\ X_\alpha \end{pmatrix} . \end{aligned} \tag{1}$$

Here, X_α denotes the new $U(1)_{L_\mu - L_\tau}$ gauge boson, while $B_{\alpha\beta}$, $W^3_{\alpha\beta}$ and $X_{\alpha\beta}$ are the hypercharge, neutral $SU(2)_L$ and $U(1)_{L_\mu - L_\tau}$ field strengths, respectively. Furthermore, $g_{\mu\tau}$ is the $U(1)_{L_\mu - L_\tau}$ gauge coupling, and ϵ_B and ϵ_W are the kinetic mixing parameters with the hypercharge and neutral weak boson, respectively. Note that the mixing of the $U(1)_{L_\mu - L_\tau}$ boson with the neutral weak component, $\epsilon_W/2\, W^3_{\alpha\beta} X^{\alpha\beta}$, is generated at the one-loop level from the $SU(2)_L$ lepton doublets running in the loop [59]. The new gauge boson X_α couples to SM leptons through the gauge current

$$j^\alpha_{\mu\tau} = \bar{L}_2 \gamma^\alpha L_2 + \bar{\mu}_R \gamma^\alpha \mu_R - \bar{L}_3 \gamma^\alpha L_3 - \bar{\tau}_R \gamma^\alpha \tau_R\,. \tag{2}$$

The lack of any gauge interactions with conventional matter composed of electrons and quarks (and thus hadrons) sets this gauge group apart from other anomaly-free $U(1)$ extensions. At the one-loop level, however, the coupling of the leptophilic gauge boson to the leptons induces an interaction with all SM fermions via a kinetic mixing term with the SM photon and Z boson. At energies $E \sim T_{\rm WD} \ll m_{\mu,\tau}$, we find for these mixings (cf. Appendix 1 for details)

$$\epsilon_A = \frac{e\,g_{\mu\tau}}{6\pi^2}\,\log\left(\frac{m_\mu}{m_\tau}\right) \sim -\frac{g_{\mu\tau}}{70}\,, \tag{3}$$

$$\epsilon_Z = -\frac{1}{2}\frac{s_W}{c_W}\epsilon_A\,, \tag{4}$$

where s_W and c_W are the sine and cosine of the Weinberg angle θ_W. These irreducible loop-induced kinetic mixings are finite and effectively lead to loop-suppressed interactions of the $U(1)_{L_\mu - L_\tau}$ boson with quarks and electrons.

In the physical mass basis of the dark photon A', we can express the interactions of the new mediator as (cf. Appendix 2),

$$\mathcal{L}_{\rm int} = -g_{\mu\tau}\, j^\alpha_{\mu\tau}\, A'_\alpha + e\,\epsilon_A \left(j^\alpha_{\rm EM} - \frac{1}{2}\tan^2\theta_W\, j^\alpha_Z \right) A'_\alpha\,, \tag{5}$$

[1] Cancelling the gauge anomalies of $U(1)_{B-L}$ requires the addition of three right-handed, SM-singlet neutrinos. The groups $U(1)_{L_i - L_j}$ are already anomaly-free without the addition of right-handed neutrinos (if Majorana mass terms for the neutrinos are forbidden [7]).

[2] As noted in Ref. [58], however, explanations of the H_0 tension by light vector mediators are not able to account for the less severe tension in the cosmological parameter σ_8 linked to the small scale power spectrum of the universe.

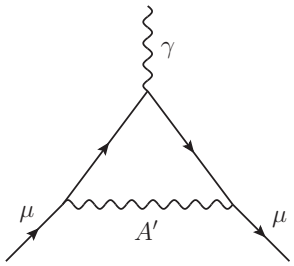

FIG. 1. Loop contribution of the $U(1)_{L_\mu - L_\tau}$ boson to the muon anomalous magnetic moment $(g-2)_\mu$.

with the electromagnetic and Z current defined as

$$j^\alpha_{\rm EM} = \sum_f Q^{\rm EM}_f \, \bar{f}\gamma^\alpha f \,, \tag{6}$$

$$j^\alpha_Z = \sum_f \bar{f}\,\gamma^\alpha \, \frac{1}{2}\left[(T^3_f - 2\,s^2_W\,Q^{\rm EM}_f) - T^3_f\,\gamma^5\right] f \,. \tag{7}$$

From Eq. (5) we see that the mass eigenstate of the $U(1)_{L_\mu - L_\tau}$ boson acquires couplings to the SM electromagnetic and Z currents suppressed by the kinetic mixing parameter ϵ_A.

II.1. Muon anomalous magnetic moment

Due to its gauge interactions with the second-generation leptons the $U(1)_{L_\mu - L_\tau}$ gauge boson A' contributes to the anomalous magnetic moment of the muon, $a_\mu = (g-2)_\mu/2$, via the loop process displayed in Fig. 1. For any neutral gauge boson with vectorial couplings to muons (as in $U(1)_{L_\mu - L_\tau}$), the additional contribution to a_μ can be expressed in the compact form [60, 61],

$$\Delta a_\mu = Q'^2_\mu \, \frac{\alpha'}{\pi} \int_0^1 du \, \frac{(1-u)\,u^2}{u^2 + \dfrac{(1-u)}{x^2_\mu}} \,, \tag{8}$$

where $\alpha' = g^2_{\mu\tau}/4\pi$, $x_\mu = m_\mu/m_{A'}$ and Q'_μ denotes the $U(1)_{L_\mu - L_\tau}$ charge of the muon.

In recent years, there has been significant theoretical effort to improve the precision of the SM prediction of $(g-2)_\mu$ [62], with the current theoretical result being

$$a^{\rm SM}_\mu = 116\ 591\ 810(43) \times 10^{-11} \,. \tag{9}$$

At the same time, the E989 experiment at Fermilab has recently reported results from their runs 2 and 3, determining the value of $(g-2)_\mu$ with unprecedented levels of precision [63]. Combined with their run-1 result [64] and the previous BNL result [65], the current experimental world average amounts to

$$a^{\rm exp}_\mu = 116\ 592\ 059(22) \times 10^{-11} \,. \tag{10}$$

This leads to a $\sim 5.2\sigma$ excess of the experimentally observed value from the theoretical prediction in Eq. (9) captured by the total deviation of

$$\Delta a_\mu = 249(48) \times 10^{-11} \,. \tag{11}$$

The preferred region in parameter space, where the contribution of a $U(1)_{L_\mu - L_\tau}$ boson to $(g-2)_\mu$ can account for this excess is shown by the green band in Fig. 5.

It should be noted that a recent lattice result of the leading-order hadronic vacuum polarisation [66] significantly decreases the above tension. This, however, comes at the cost of worsening fits to other electroweak precision observables [67].

III. WHITE DWARF COOLING

In this section, we outline the computation of the WD luminosity in neutrinos under the addition of a novel $U(1)_{L_\mu - L_\tau}$ gauge boson. In doing so we follow closely the computation of Ref. [68]. Importantly, we carefully develop the relevant expressions for a light leptophilic gauge boson where plasma effects play a relevant role. We consider a hot white dwarf, in which the main source of energy loss is plasmon decay. We also regard a $U(1)_{L_\mu - L_\tau}$ leptophilic dark photon that contributes to the plasmon decay. This novel vector mediator has different contributions for each flavour of neutrino-antineutrino pairs that are emitted in the plasmon decay process. In order to obtain more compact expressions, we will introduce the following definitions encapsulating the A' couplings to electrons and neutrinos,

$$d^e_V = e\,\epsilon_A\Big(1 - \tan^2\theta_W(1 - 4\sin^2\theta_W)/8\Big) \,, \tag{12}$$

$$d^e_A = e\,\epsilon_A\ \tan^2\theta_W/8 \,, \tag{13}$$

$$k^\alpha_\nu = s_\alpha\, g_{\mu\tau}/2 + d^e_A \,, \tag{14}$$

where $s_\alpha = 0, 1, -1$ for $\alpha = e, \mu, \tau$, respectively. The contribution to the neutrino emissivity of a WD due to a novel $U(1)_{L_\mu - L_\tau}$ boson originates from the diagram of Fig. 2, which is identical to the SM neutral current contribution but with a dark photon A' instead of the SM Z. Due to

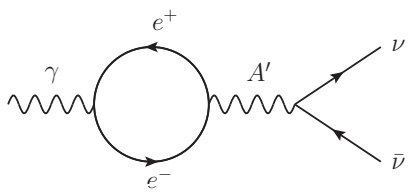

FIG. 2. Plasmon decay contribution via $U(1)_{L_\mu - L_\tau}$ boson coupling to electrons via kinetic mixing.

the kinetic mixing coupling of the dark photon to electrons in this model, the BSM contribution can be calculated exactly analogous to the SM Z. Hence, we only need to redefine the values of C_V and C_A for each neutrino flavour in Eqs. (36-38) of Ref. [69] and consider the full expression for the dark photon propagator to allow for A' masses comparable to the WD plasma frequency,

$$C_a^{\alpha,\mathrm{SM+BSM}}(q) \to C_a^\alpha + b_a \frac{\sqrt{2}}{G_F} \frac{k_\nu^\alpha \, d_a^e}{q^2 - m_{A'}^2} \,, \quad (15)$$

where $a = V, A$ are the vectorial and axial components with $b_V = 1$ and $b_A = -1$. Here, q is the 4-momentum of the plasmon, α denotes the flavour of the SM neutrino final states, and C_a^α are the coefficients obtained from the SM plasmon decay diagrams: the vectorial ones are equal to $2\sin^2\theta_W + 0.5$ (for e) and $2\sin^2\theta_W - 0.5$ (for μ and τ), and the axial are 0.5 (for e) and -0.5 (for μ and τ). With this, the WD emissivities into neutrino-antineutrino pairs can be written as

$$\begin{aligned}\mathcal{Q}_L =& \frac{G_F^2}{96\pi^4\alpha}\int_0^\infty d|\boldsymbol{q}| \sum_\alpha (C_V^{\alpha,\mathrm{SM+BSM}}(q))^2 \, \boldsymbol{q}^2 \, Z_l(\boldsymbol{q}) \\ &\times \left(\omega_l(\boldsymbol{q})^2 - \boldsymbol{q}^2\right)^2 \omega_l(\boldsymbol{q})^2 \, n_B(\omega_l(\boldsymbol{q})) \,, \end{aligned} \quad (16)$$

$$\begin{aligned}\mathcal{Q}_T =& \frac{G_F^2}{48\pi^4\alpha}\int_0^\infty d|\boldsymbol{q}| \sum_\alpha (C_V^{\alpha,\mathrm{SM+BSM}}(q))^2 \, \boldsymbol{q}^2 \, Z_t(\boldsymbol{q}) \\ &\times \left(\omega_t(\boldsymbol{q})^2 - \boldsymbol{q}^2\right)^3 n_B(\omega_t(\boldsymbol{q})) \,, \end{aligned} \quad (17)$$

$$\begin{aligned}\mathcal{Q}_A =& \frac{G_F^2}{48\pi^4\alpha}\int_0^\infty d|\boldsymbol{q}| \sum_\alpha (C_A^{\alpha,\mathrm{SM+BSM}}(q))^2 \, \boldsymbol{q}^2 \, Z_t(\boldsymbol{q}) \\ &\times \left(\omega_t(\boldsymbol{q})^2 - \boldsymbol{q}^2\right) \Pi_A\left(\omega_t(\boldsymbol{q}), \boldsymbol{q}\right)^2 \, n_B(\omega_t(\boldsymbol{q})) \,, \end{aligned} \quad (18)$$

where the boldface $\boldsymbol{q}$ denotes the 3−momentum of the dark photon, $n_B(\omega)$ is the Bose-Einstein distribution function and the subscripts L, T, A denote the longitudinal, transverse and axial contributions, respectively. The WD luminosity due to neutrinos is obtained by integrating the emissivities over the volume of the WD core. Considering spherical symmetry, the luminosity is obtained as

$$L_{\mathrm{WD}} = 4\pi \int_0^{R_{\mathrm{WD}}} \mathcal{Q}_{tot} \, r^2 dr \,, \quad (19)$$

where R_{WD} is the radius of the WD. For our computations, we have chosen a representative value of $M_{\mathrm{WD}} = 1\, M_\odot$ for the mass of the WD. However, the results are not altered by picking smaller values. If the star has a temperature of $T_{\mathrm{WD}} \gtrsim 10^{7.8}$ K then the photon luminosity is just $L_\gamma \gtrsim 10^{-0.5} L_\odot$ [70] and the main cooling mechanism is the plasmon decay inside the star. Therefore, at these temperatures, extra contributions to plasmon decay have an impact on the overall cooling. The limits are computed by estimating the relative excess contribution, $\varepsilon^{\mathrm{BSM}}$, of the novel $U(1)_{L_\mu - L_\tau}$ boson over the SM one,

$$\varepsilon^{\mathrm{BSM}} \equiv \left(L_{\mathrm{WD}}^{\mathrm{SM+BSM}} - L_{\mathrm{WD}}^{\mathrm{SM}}\right) / L_{\mathrm{WD}}^{\mathrm{SM}} \,. \quad (20)$$

In the following, we discuss the three regimes of dark photon masses with respect to the WD temperatures:

(1) The *heavy regime* with $m_{A'} \gg T_{\mathrm{WD}}$.

(2) The *ultra-light regime* with $m_{A'} \ll T_{\mathrm{WD}}$.

(3) The *resonant regime* with $m_{A'} \sim T_{\mathrm{WD}}$.

III.1. Heavy dark photons

A WD cannot reach temperatures for which the energies of the plasmon decay are substantially greater than $\mathcal{O}(10)$ MeV. Therefore, in the heavy regime of $m_{A'} \gtrsim 10$ MeV the dark photon propagator entering the momentum-integral in the emissivity can be well approximated as $1/(q^2 - m_{A'}^2) \sim -1/m_{A'}^2$. Hence, $C_V^{\alpha,\mathrm{SM+BSM}}$ and $C_A^{\alpha,\mathrm{SM+BSM}}$ no longer depend on q and we can directly compute $\varepsilon^{\mathrm{BSM}}$ since the axial contribution is negligible,

$$\begin{aligned}\varepsilon^{\mathrm{BSM}} &= \sum_\alpha \left(C_V^{\alpha,\mathrm{SM+BSM}}\right)^2 / \sum_\alpha \left(C_V^{\alpha,\mathrm{SM}}\right)^2 - 1 \\ &\simeq 1.50 \times 10^{17} \left(\frac{g_{\mu\tau}}{m_{A'}/1\ \mathrm{MeV}}\right)^4 \\ &\quad - 1.66 \times 10^5 \left(\frac{g_{\mu\tau}}{m_{A'}/1\ \mathrm{MeV}}\right)^2 . \end{aligned} \quad (21)$$

This quantity is also independent of the exact temperature of the WD, but is only valid for

masses that are much greater than the plasma frequency of the WD[3]. Due to the relative smallness of ϵ_Z compared to ϵ_A, the results are also unaltered if we neglect the dark photon coupling to the Z current in Eq. (5).

III.2. Ultra-light dark photons

In the case of an ultra-light dark photon mediator, effects due to the self energy correction to the propagator become relevant when computing its propagation in the stellar medium and the subsequent plasmon decay. The dark photon self energy is given by

$$\begin{aligned}\Pi^{\mu\nu}_{A'}(q) = -\int \frac{d^4k}{(2\pi)^4}\, &\mathrm{tr}\big[\gamma^\mu(d^e_V + d^e_A\gamma^5)(\not{k} + m_{A'}) \\ &\times \gamma^\nu(d^e_V + d^e_A\gamma^5)(\not{q} - \not{k} - m_{A'})\big] \\ &\times \left\{\frac{i}{k^2 - m^2_{A'}} - 2\pi\big[\theta(-k^0)\right. \\ &\left. + \mathrm{sign}(k^0)\,\tilde{f}(k^0 - \mu)\big]\delta\big(k^2 - m^2_{A'}\big)\right\} \\ &\times \left\{\frac{i}{(q-k)^2 - m^2_{A'}} - 2\pi\big[\theta(-q^0 + k^0)\right. \\ &+ \mathrm{sign}(q^0 - k^0)\,\tilde{f}(q^0 - k^0 + \mu)\big] \\ &\left.\times\, \delta\big((q-k)^2 - m^2_{A'}\big)\right\}.\end{aligned} \tag{22}$$

where $\tilde{f}(x) \equiv (e^{\beta x} + 1)^{-1}$ with $\beta = 1/(k_B\, T)$.

We can conveniently express this in terms of the plasmon self energy $\Pi^{\mu\nu}_\gamma$. To do so, we note that $(d^e_A)^2/(d^e_V)^2 \sim \mathcal{O}(10^{-3})$ is negligible, as well as the axial contribution to the self-energy, which is $\sim d^e_V\, d^e_A\, \Pi_{A,\gamma}$. This is warranted since the axial contribution to the plasmon self-energy $\Pi_{A,\gamma}$ appearing is typically four to six orders of magnitude smaller than the longitudinal and transverse ones. Taking this into account, the final expression for the dark photon self energy reads

$$\Pi^{\mu\nu}_{A'}(q) = \frac{(d^e_V)^2 + (d^e_A)^2}{4\pi\alpha}\,\Pi^{\mu\nu}_\gamma(q)\,, \tag{23}$$

with $\Pi^{\mu\nu}_\gamma$ the plasmon self-energy. Next, we need to compute the full propagator, $D^{\mu\nu}_{A'}$, up to the same order, $\mathcal{O}(\alpha)$, used for the plasmon decay computation. To compute this quantity, we need to expand the self-energy into its longitudinal and transverse components. We can work with the same projectors as used for the photon since, as we saw, the dark photon self-energy is proportional to that of the photon. Hence, we can write

$$\Pi^{\mu\nu}_{A'} = F_{A'}\, P^{\mu\nu}_L + G_{A'}\, P^{\mu\nu}_T\,, \tag{24}$$

with the transverse and longitudinal projectors given by

$$\begin{aligned} P^{\mu\nu}_T &= \big(\delta^{ij} - \hat{q}^i\hat{q}^j\big)\,\delta^\mu_i\,\delta^\nu_j\,, \\ P^{\mu\nu}_L &= \left(-g^{\mu\nu} + \frac{q^\mu q^\nu}{q^2}\right) - P^{\mu\nu}_T\,. \end{aligned} \tag{25}$$

Here, the factors $F_{A'}$ and $G_{A'}$ are obtained analogously to the photon case, by contracting $\Pi^{\mu\nu}_{A'}$ with the projectors of Eq. (25). Formally, we can write this as

$$F_{A'} \equiv \Pi^{00}_{A'}\,\frac{q^2}{\boldsymbol{q}^2}\,, \qquad G_{A'} \equiv \Pi^{xx}_{A'}\,, \tag{26}$$

where x is any direction transverse to the propagation of the dark photon with 4−momentum $q = (\omega, \boldsymbol{q})$.

Importantly, we note that since $\Pi^{\mu\nu}_{A'}$ is proportional to the plasmon self-energy, its contraction with q^μ vanishes. Hence it is respecting the Ward identity, even though the gauge symmetry is broken. In our computation, the full propagator $D^{\mu\nu}_{A'}$ is contracted with the plasmon self-energy $\Pi^{\mu\nu}_\gamma$. Thus, we will neglect any term proportional to q^μ. Furthermore, we remind ourselves that for the projectors $P^\mu_{T\lambda}\, P^{\lambda\nu}_T = P^{\mu\nu}_T$, $P^\mu_{L\lambda}\, P^{\lambda\nu}_L = P^{\mu\nu}_L$, and $P^\mu_{L\lambda}\, P^{\lambda\nu}_T = P^\mu_{T\lambda}\, P^{\lambda\nu}_L = 0$. With these preparations, we can write the expression for the full propagator of the dark photon as

[3] See Eq. (33) for the full expression of the plasma frequency.

$$
\begin{aligned}
D^{\mu\nu}_{A'} &= \frac{-i\,(g^{\mu\nu} - q^\mu q^\nu/m^2_{A'})}{q^2 - m^2_{A'}} + \frac{-i\,(g^\mu_\lambda - q^\mu q_\lambda/m^2_{A'})}{q^2 - m^2_{A'}}\,(i\,\Pi^{\lambda\sigma}_{A'})\,\frac{-i\,(g^\nu_\sigma - q_\sigma q^\nu/m^2_{A'})}{q^2 - m^2_{A'}} + \ldots \\
&= \frac{-i\,g^{\mu\lambda}}{q^2 - m^2_{A'}}\left[\delta^\nu_\lambda + \sum_{n=1}^{\infty}\left(\frac{F_{A'}}{q^2 - m^2_{A'}}\right)^n P^\nu_{L\lambda} + \sum_{n=1}^{\infty}\left(\frac{G_{A'}}{q^2 - m^2_{A'}}\right)^n P^\nu_{T\lambda}\right] \\
&= \frac{-i\,g^{\mu\lambda}}{q^2 - m^2_{A'} - F_{A'}}\,P^\nu_{L\lambda} + \frac{-i\,g^{\mu\lambda}}{q^2 - m^2_{A'} - G_{A'}}\,P^\nu_{T\lambda}\,,
\end{aligned}
\tag{27}
$$

where finally we have

$$
F_{A'} \equiv \frac{(d^e_V)^2 + (d^e_A)^2}{4\pi\alpha}\,\frac{q^2}{\boldsymbol{q}^2}\,\Pi^\gamma_L\,, \tag{28}
$$

$$
G_{A'} \equiv \frac{(d^e_V)^2 + (d^e_A)^2}{4\pi\alpha}\,\Pi^\gamma_T\,, \tag{29}
$$

with Π^γ_L and Π^γ_T the plasmon longitudinal and transverse self-energies, that can be found in [68] in Eqs. (18) and (19). To obtain the last line of Eq. (27), we have made use of the identity

$$
\delta^{\lambda\nu} = P^{\lambda\nu}_L + P^{\lambda\nu}_T + q^\lambda q^\nu/q^2\,. \tag{30}
$$

In the computation of the emissivities the full A' propagator $D^{\mu\nu}_{A'}$ is contracted with the plasmon self-energy $\Pi^{\mu\nu}_\gamma$. Hence, we find that only the longitudinal component of $D^{\mu\nu}_{A'}$ enters the longitudinal emissivity and only its transverse component enters the transverse and axial emissivities. Furthermore, since the A' self-energy can be expressed in terms of the photon self-energy and the 4-momentum at which it is evaluated is the on-shell plasmon momentum (due to momentum conservation), we can use the standard plasmon relations to evaluate $P^{\mu\nu}_L$ and $P^{\mu\nu}_T$ for the dark photon. Taking this into consideration, the expression for the full propagator finally simplifies to

$$
\begin{aligned}
D^{\mu\nu}_{A'} =& \frac{-i\,P^{\mu\nu}_L}{q^2 - m^2_{A'} - \dfrac{(d^e_V)^2 + (d^e_A)^2}{4\pi\alpha}\left(\omega_l(\boldsymbol{q})^2 - \boldsymbol{q}^2\right)} \\
&+ \frac{-i\,P^{\mu\nu}_T}{q^2 - m^2_{A'} - \dfrac{(d^e_V)^2 + (d^e_A)^2}{4\pi\alpha}\left(\omega_t(\boldsymbol{q})^2 - \boldsymbol{q}^2\right)}\,.
\end{aligned}
\tag{31}
$$

This expression for the full propagator has to be used instead of the naive tree-level propagator $\frac{-i}{q^2 - m^2_{A'}}$ in computing the coupling coefficients in Eq. (15). Effectively, this means that in the computation of the longitudinal emissivity the denominator of the coefficient $C^{\alpha,\mathrm{SM+BSM}}_V(q)$ has to be replaced by the one of the first term in Eq. (31). Similarly, for the transverse and axial components the denominator of the coupling coefficients $C^{\alpha,\mathrm{SM+BSM}}_V(q)$ and $C^{\alpha,\mathrm{SM+BSM}}_A(q)$ have to be replaced by the denominator of the second term in Eq. (31).

In the very low mass region, where $m^2_{A'} \ll q^2$, the luminosities become approximately independent of the mass. To see this, let us consider the denominator of the propagator in Eq. (31). This has the form $(1 - r_{\mathrm{BSM}})\,q^2 - m^2_{A'}$, where $r_{\mathrm{BSM}} \equiv \left[(d^e_V)^2 + (d^e_A)^2\right]/4\pi\alpha$. Since $r_{\mathrm{BSM}} \ll 1$, in this region the denominator of the propagator can be approximated as $\sim 1/q^2$. The luminosity in this region is then obtained by integrating the emissivities in Eqs. (16) to (18) with the replacements,

$$
\begin{aligned}
\sum_\alpha (C^{\alpha,\mathrm{SM+BSM}}_V(q))^2 &= \frac{d^V_e}{G^2_F\,(q^2_r)^2}\left(d^V_e\left(6\,(d^A_e)^2 + g^2_{\mu\tau}\right) + \sqrt{2}\,G_F\,q^2_r\left[2\,d^A_e\sum_\alpha C^{\alpha,\mathrm{SM}}_V + g_{\mu\tau}\left(C^{\mu,\mathrm{SM}}_V - C^{\tau,\mathrm{SM}}_V\right)\right]\right) \\
\sum_\alpha (C^{\alpha,\mathrm{SM+BSM}}_A(q))^2 &= \frac{d^A_e}{G^2_F\,(q^2_r)^2}\left(6\,(d^A_e)^3 - \sqrt{2}\,G_F\,g_{\mu\tau}\left(C^{\mu,\mathrm{SM}}_A - C^{\tau,\mathrm{SM}}_A\right)q^2_r + G_F\,d^A_e\left[g^2_{\mu\tau} - 2\sqrt{2}\,G_F\,q^2_r\sum_\alpha C^{\alpha,\mathrm{SM}}_A\right]\right)
\end{aligned}
\tag{32}
$$

where we have defined $q^2_r \equiv (1 - r_{\mathrm{BSM}})\,q^2$.

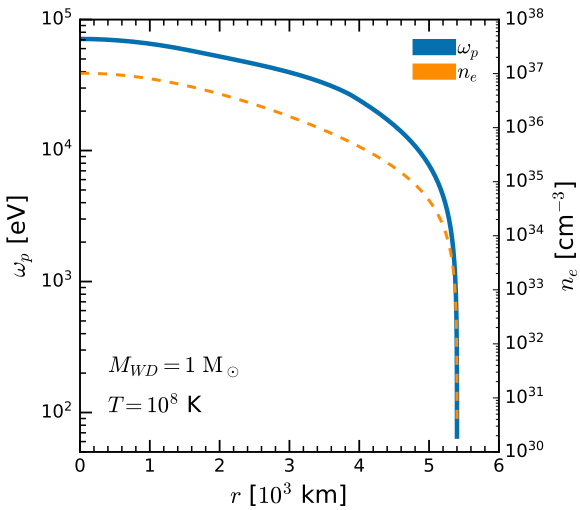

FIG. 3. Plasma frequency ω_p (blue line) and electron density n_e (orange dashed line) of a WD with $M_{\rm WD} = 1 M_\odot$ at $T_{\rm WD} = 10^8$ K as a function of the distance to the centre of the star in km.

III.3. Resonant dark photons

When the dark photon mass is roughly of the same order as the WD temperature of $\mathcal{O}$(keV)[4] the A' contribution to the WD emissivities are significantly enhanced due to a resonance in the A' propagator. More precisely, this happens when the dark photon mass hits the plasma frequency, which is defined as [69]

$$\omega_p^2 = \frac{4\alpha}{\pi}\int_0^\infty d|\boldsymbol{k}|\frac{\boldsymbol{k}^2}{E_k}\left(1-\frac{1}{3}v^2\right)\left(f_e(E_k)+f_{\bar{e}}(E_k)\right), \tag{33}$$

where f_e and $f_{\bar{e}}$ are the Fermi thermal distributions for electrons and positrons, respectively. We are integrating over the 3−momentum of the electrons and positrons in the plasma with energy $E_k \equiv \sqrt{\boldsymbol{k}^2+m_e^2}$ and velocity $v \equiv \boldsymbol{k}/E_k$. The plasma frequency ω_p depends on the temperature $T_{\rm WD}$ and the chemical potential μ, which in turn depends on the distance r from the centre of the WD.

In Fig. 3, we show the plasma frequency ω_p and electron density n_e as a function of the WD radius r. We can see that the plasma frequency reaches its maximum at the centre of the star and decreases roughly over an order of magnitude throughout the interior of the star before it rapidly drops in the outer layers. This behaviour can be readily understood by looking at the electron density profile since the plasma frequency ω_p is directly proportional to it.

Thus, the resonance region consists of a whole range of dark photon masses for which a pole arises in the A' propagator due to the scanning of the plasma frequency ω_p in the range $0 \le r \le R_{\rm WD}$. This effect, if not cured, leads to a continuous curve of divergences of the integrands in Eqs. (16) to (18) in the $|\boldsymbol{q}| - r$ plane, where $\boldsymbol{q}$ is the 3−momentum of the external plasmon and r the distance from the centre of the WD.

However, these divergences are non-physical and can be cured by considering the Breit-Wigner (BW) propagator [71]. This takes into account the imaginary component of the self-energy, which is directly related to the instability of the particle, and therefore is closely related to its decay width. The BW propagator takes the form [72]

$$G^{\mu\nu}_{\rm BW}(q^2) = \frac{-i(g^{\mu\lambda}-q^\mu q^\lambda/m^2)}{q^2-m^2-{\rm Re}(F)-i\,{\rm Im}(F)}P^\nu_{L\lambda} + \frac{-i(g^{\mu\lambda}-q^\mu q^\lambda/m^2)}{q^2-m^2-{\rm Re}(G)-i\,{\rm Im}(G)}P^\nu_{T\lambda}\,, \tag{34}$$

where the self-energy of the vector is $\Pi^{\mu\nu} = F\,P_L^{\mu\nu} + G\,P_T^{\mu\nu}$, in terms of the projectors $P_L^{\mu\nu}$ and $P_T^{\mu\nu}$ given in Eq. (25).

There are, in principle, two main contributions to the imaginary part of the dark photon self energy ${\rm Im}(\Pi_{A'})$. The first one is due to a thermal loop of electrons, while the second one is due to a zero-temperature loop of neutrinos, since neutrinos are not thermalized inside the WD star. In the resonance region of masses $m_{A'} \ll 1$ MeV, there is no imaginary contribution from the electron loop since the dark photon is not massive enough to decay into an electron-positron pair. It can, however, decay into a pair of neutrino-antineutrino, which for the corresponding A' masses and WD temperatures can be considered to be massless. We have to include the imaginary contributions $i\,{\rm Im}(\Pi_{A',\lambda})$ in the propagators of each polarisation $\lambda = T, L$ in Eq. (31).

After renormalizing the self-energy with internal neutrinos of flavour α using the $\overline{\rm MS}$ scheme, we obtain the following expressions,

$$\bar{\Pi}^{\mu\nu}_{A'}(q^2) = -\frac{\left(k_\nu^\alpha\right)^2}{4\pi^2}q^2 g^{\mu\nu}\int_0^1 dx\,x\,(1-x) \times \log\left(\frac{m_\alpha^2}{m_\alpha^2 - x(1-x)q^2}\right), \tag{35}$$

[4] In the computations a temperature of $T_{\rm WD} = 10^8$ K was used.

where k_ν^α is the coefficient defined in Eq. (12). In the limit of massless neutrinos, the imaginary part of this self-energy is easily found as the argument of the logarithm is always negative in the region of integration, since in turn the momentum of the thermal on-shell plasmon, q^2, is always positive. Hence, we find

$$\begin{aligned}\mathrm{Im}(\bar{\Pi}^{\mu\nu}_{A'})(q^2) &= \frac{\left(k_\nu^\alpha\right)^2}{24\pi} q^2 g^{\mu\nu} \\ &= \frac{\left(k_\nu^\alpha\right)^2}{24\pi} \frac{(\omega_l^2 - \boldsymbol{q}^2)^2}{\boldsymbol{q}^2} P_L^{\mu\nu} \\ &\quad - \frac{\left(k_\nu^\alpha\right)^2}{24\pi} (\omega_t^2 - \boldsymbol{q}^2) P_T^{\mu\nu} \,,\end{aligned} \tag{36}$$

where we have replaced q^2 by its explicit value for the two polarizations.

Finally, the quantities entering the denominators of the dark photon propagator in Eq. (34), following the same procedure as in Section III.2, are $\mathrm{Im}(F) = \mathrm{Im}(\bar{\Pi}^{00}_{A'}) \times q^2/\boldsymbol{q}^2$ and $\mathrm{Im}(G) = \mathrm{Im}(\bar{\Pi}^{xx}_{A'})$ for the longitudinal and transverse polarisation, respectively. The projectors are absorbed when multiplied by those of the electronic loop of the plasmon. To obtain the full expression we still have to sum over the different neutrino flavours α in $\mathrm{Im}(\bar{\Pi}^{\mu\nu}_{A'})$, $k_\nu^\alpha \to \sum_\alpha k_\nu^\alpha$.

This prescription regulates the divergences in the dark photon propagator and leads to finite expressions in the whole parameter space. Nevertheless, the curve of very narrow peaks in the $|\boldsymbol{q}| - r$ plane of integration remains. To reliably evaluate the luminosity integrals in this regime, we have to thoroughly sample these narrow peaks, for which we were relying on the `VEGAS+` algorithm [73] for adaptive multidimensional Monte Carlo integration in our calculations.

IV. RESULTS

In the following, we present our results for WD cooling via plasmon decay in presence of a $U(1)_{L_\mu - L_\tau}$ gauge boson. The results were derived for a representative WD with a mass of $M_{\mathrm{WD}} = 1\ M_\odot$, a temperature of $T_{\mathrm{WD}} = 10^8$ K, and the profiles of the electron number density n_e and chemical potential μ obtained from solving the Salpeter EoS [36]. For the numerical computation of the self-energy, we have considered two main approximations. For the inner layers of the WD, we considered a degenerate regime, where the chemical potential μ dominates over the temperature T_{WD} and mass of the electron. The quantities depend mainly on the Fermi momentum in this regime. For the outer layers, we regarded the classical regime, where the mass of the electron dominates over the temperature and over the sum of the chemical potential and temperature. In this regime, the quantities depend mainly on the electron number density n_e. More details on these limits and their respective expressions can also be found in [36].

In Fig. 4 we present the general behaviour of the WD cooling sensitivities to plasmon decay by an extra $U(1)_{L_\mu - L_\tau}$ boson obtained via the computations outlined in Section III. Current best fits of the hot WD luminosity function allow for a variation of the neutrino luminosity function with respect to the SM by a scaling factor of $0.6 \lesssim f_s \lesssim 1.7$ at the 95 % confidence level (CL) [74]. Therefore, an exclusion of more than $\varepsilon^{\mathrm{BSM}} = 30\,\%$ (red line) excess cooling at the 90 % CL by a future observation of hot young WDs seems realistic. We show the sensitivity line in the $m_{A'} - g_{\mu\tau}$ plane of $\varepsilon^{\mathrm{BSM}} = 0.3$ extra cooling relative to the SM, as defined in Eq. (20). This plot illustrates well the three qualitatively different domains of WD cooling depending on the A' mass already outlined throughout the paper.

For heavy dark photon masses of $m_{A'} \gtrsim 10^5$ eV, we observe a linear scaling of the sensitivity line. This is readily explained by looking at the WD plasma frequency in Fig. 3. Throughout the star the plasma frequency assumes its maximum value at $\omega_{p,\max} \lesssim 10^5$ eV. Hence, for dark photon masses above $\omega_{p,\max}$ the A' propagator in the emissivity is entirely dominated by its mass and scales as $\sim 1/m_{A'}^2$. The linear increase can be understood from the solution of the approximation in Eq. (21).

On the other hand, for ultra-light dark photons instead, we see a constant scaling of the sensitivity independent of the dark photon mass. This can be understood by an inspection of the propagator of the dark photon. As we stated in section Section III.2, for ultra-light dark photons with $m_{A'} \ll q$ much smaller than the typical momenta in the stellar interior, we can well approximate the propagator in the WD emissivities by $\sim 1/q^2$. Hence, in this very light regime the WD sensitivity becomes independent of the A' mass to excellent approximation.

Finally, we will discuss the central region of the plot where the resonance behaviour dominates. For masses of the order of the plasma frequency, ω_p, there is a resonance in the propagator between the dark photon mass $m_{A'}$ and the momentum transfer q. As can be seen in Fig. 3, as soon as

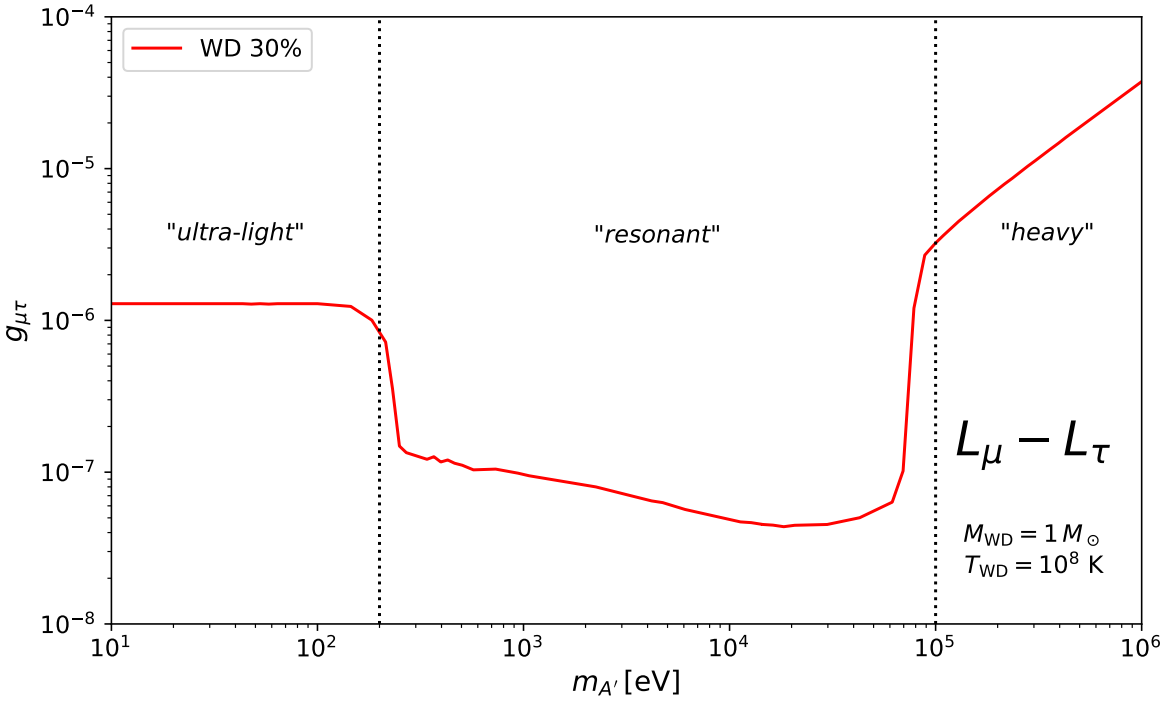

FIG. 4. WD cooling bounds on sub-MeV $U(1)_{L_\mu - L_\tau}$ bosons. At high dark photon masses of $m_{A'} \gtrsim 100$ keV, the A' propagator in the WD emissivities is dominated by the A' mass and is to good approximation independent of the plasma frequency ω_p. Below this threshold the A' mass scans the plasma frequency in different phase space regions, leading to a resonance behaviour in the window of 0.2 keV $\lesssim m_{A'} \lesssim$ 100 keV. At the low-mass end of this window the resonance peaks of the BW propagator start slowly moving outside the integration domain of the luminosity $L_{\rm WD}$ towards higher radii $r > R_{\rm WD}$ resulting in an attenuation of the resonance. Below $m_{A'} \lesssim 200$ eV the integrand no longer exposes any resonance behaviour in the integration domain and the integrand is dominated by the plasma frequency and approximately independent of the A' mass.

the dark photon masses fall below the maximum plasma frequency of $\omega_{p,\rm max} \lesssim 10^5$ eV, resonance will occur in some region in the interior of the star. This explains why the transition between the linear and resonant regime is so abrupt. Due to the Breit-Wigner prescription, this resonance will produce large narrow, but regulated peaks in the integrand of the emissivity. Since these peaks contribute significantly to the integral, they are largely enhancing the sensitivity of WD cooling to a new $U(1)_{L_\mu - L_\tau}$ boson. As the dark photon masses decrease, the location of these peaks within the integration domain will shift towards higher and higher radii. For masses below about ~ 300 eV these peaks will start moving past the WD radius $R_{\rm WD}$ and out of the integration domain. Hence, their contribution becomes less and less important until no resonance occurs at all for masses of $m_{A'} \lesssim 200$ eV and the ultra-light regime is reached.

In Fig. 5 we show the WD sensitivities on a $U(1)_{L_\mu - L_\tau}$ boson in the MeV mass window, where a solution of the muon $(g-2)_\mu$ anomaly is still allowed. For comparison, we show the current best limits in grey. At masses below $\mathcal{O}(10)$ MeV the dark photon A' contributes significantly to the heating of the neutrino gas in the early universe leading to a too large number of neutrino degrees of freedom, $\Delta N_{\rm eff}$, during BBN [20]. However, in the mass window of $m_{A'} \sim 10 - 20$ MeV the same effect leads to a milder contribution to $N_{\rm eff}$, which could explain the Hubble tension [20]. The corresponding favoured region is depicted by the blue band labeled H_0. In turn, the green band shows the region of parameter space preferred by the $(g-2)_\mu$ anomaly as measured at the E989 experiment [63] and explained in Section II.1. The most stringent constraint on the $(g-2)_\mu$ favoured region is due to the recently reported result of the invisible search at the NA64μ experiment [75]. At low masses constraints from the measurement of the ^{7}Be solar neutrino flux at the Borexino ex-

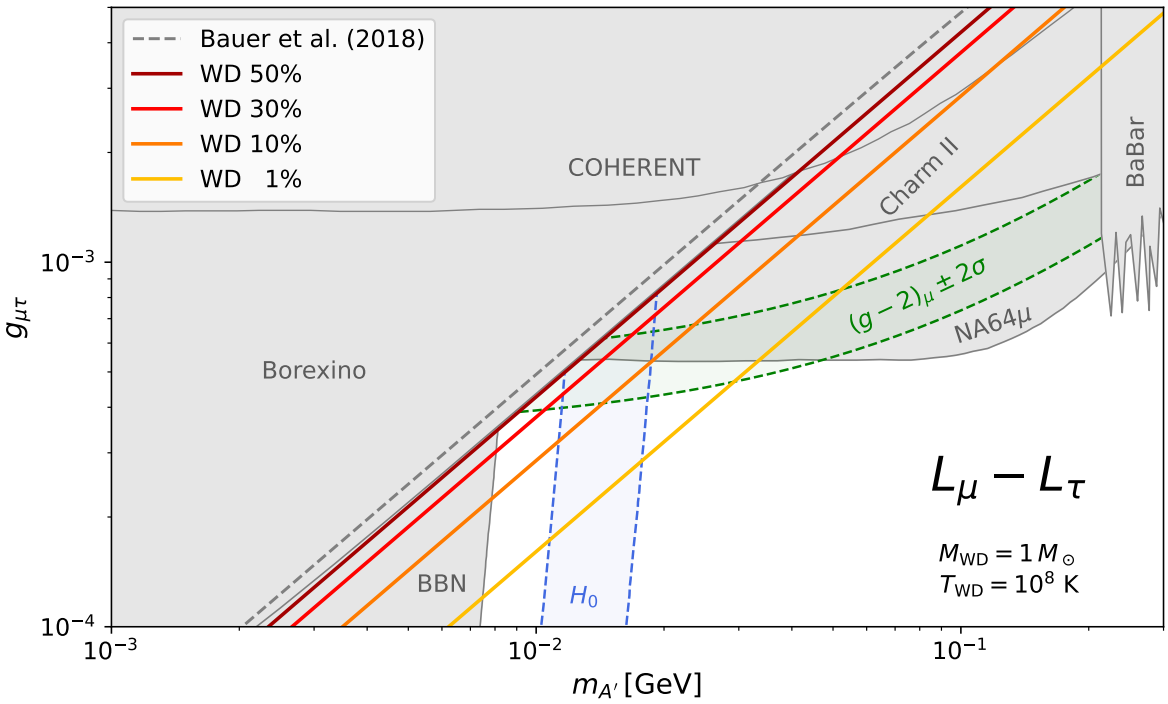

FIG. 5. Limits on MeV-mass $U(1)_{L_\mu - L_\tau}$ gauge bosons. The grey shaded areas show the current constraints (see text for explanations). The green and blue bands depict the regions of parameter space preferred by the $(g-2)_\mu$ and H_0 anomaly, respectively. We show our constraints from white dwarf cooling via plasmon decay for an excess of 50% (crimson), 30% (red), 10% (orange) and 1% (yellow) over the SM neutrino cooling rate. The grey dashed line shows the previously estimated WD cooling bound of Ref. [54].

periment [30, 76, 77] exclude a solution below A' masses of $m_{A'} \sim 10$ MeV. At high masses, we also show the limit obtained from resonance searches in four-muon production by the BaBar collaboration [78]. For comparison, we also show the resulting bound from measurements of coherent elastic neutrino-nucleus scattering (CEνNS) with a CsI[Na] target at the COHERENT experiment [79, 80]. Similarly, a strong constraint arises from the search for neutrino trident production [81]. We show the leading bound by the CHARM-II experiment [82].[5]

The crimson, red, orange and yellow lines represent our bounds obtained under the assumption of a sensitivity to $\varepsilon^{\rm BSM} = 50\%, 30\%, 10\%$ and 1% WD excess neutrino cooling over the SM prediction, respectively. For comparison, the grey dashed line shows the estimate of the WD cooling bound that has been obtained in Ref. [54] from matching to the EFT coefficients used in the analysis of [55], which in turn assumed a 100% excess cooling constraint.

First of all, we note that the conservative (crimson) 50% line lies marginally below the current best limit provided by Borexino. A realistic 30% exclusion limit would already rule out currently still allowed regions of the parameter space, where a simultaneous explanation of the $(g-2)_\mu$ and H_0 anomalies are possible. If in turn future analyses would significantly improve their sensitivity to extra neutrino cooling (via an improved extraction of the luminosity function), sensitivities at the level of 10% (orange line) excess cooling could rule out almost all of the joint $(g-2)_\mu$ and H_0 explanation, while sensitivities at the level of 1% (yellow line) would exclude almost the entire parameter space favoured by the $(g-2)_\mu$ anomaly.

[5] In principle, a more stringent bound can be derived from the CCFR results [81]. However, some doubts have been shed on the correct incorporation of a background due to diffractive charm production in the relevant analysis [83] and hence we abstain from showing the corresponding limit.

V. CONCLUSIONS

In this article, we have performed for the first time an *ab initio* computation of the WD luminosity due to plasmon decay into neutrinos in presence of an extra new $U(1)_{L_\mu - L_\tau}$ gauge boson. We have performed the calculations for a representative WD star with a mass of $M_{\rm WD} = 1 M_\odot$ and temperature of $T_{\rm WD} = 10^8$ K. Following [69], we have considered two main approximations: the degenerate regime (for the inner layers of the WD) and the classical regime (for the outer ones).

Our main result is that, given a realistic observation of the neutrino luminosity of a hot young WD at the 30% level, the resulting WD cooling bounds can exclude currently untested regions of parameter space, where a simultaneous explanation of the $(g-2)_\mu$ and H_0 anomaly are still possible (cf. Fig. 5). For a precision observation at the 10% or even 1% level, this could exclude a large fraction or even all of the remaining allowed parameter space for the $(g-2)_\mu$ anomaly in this model.

Second, we have carefully derived and computed the neutrino luminosity in the resonant regime where the A' masses are comparable to the plasma frequency ω_p. We have demonstrated that the varying profile of the electron density n_e and chemical potential μ in the interior of the star result in a broad range of A' masses of $100\ \text{eV} \lesssim m_{A'} \lesssim 100\ \text{keV}$, in which plasma resonance effects become important and lead to a significantly increased cooling contribution of the A'.

A straightforward extension of this work would be to perform the same calculations for neutron stars. However, the lack of knowledge of the precise equation of state for these stars makes it fundamentally more difficult to obtain robust results for the corresponding luminosities. Nevertheless, compared to WDs these objects exhibit much higher densities and at their birth also much higher temperatures of up to $T \sim 50$ MeV. This could significantly enhance the effect of neutrino cooling through a novel $U(1)_{L_\mu - L_\tau}$ boson and in particular improve sensitivities at higher boson masses. Furthermore, resonances at a higher mass range could result in limits improving over current ones for mediators like leptophilic dark photons.

ACKNOWLEDGEMENTS

We would like to thank Maura E. Ramirez-Quezada for the profiles of the white dwarf used for the computation of the luminosities of this paper. We also want to acknowledge the `VEGAS+` package [84] for multidimensional Monte Carlo integration. This research project was made possible through the access granted by the Galician Supercomputing Center (CESGA) to its supercomputing infrastructure. The supercomputer FinisTerrae III and its permanent data storage system have been funded by the Spanish Ministry of Science and Innovation, the Galician Government and the European Regional Development Fund (ERDF).

The work of PF was supported by the Spanish Agencia Estatal de Investigación through the grants PID2021-125331NB-I00 and CEX2020-001007-S, funded by MCIN/AEI/10.13039/501100011033. The research of JHZ has received support from the European Union's Horizon 2020 research and innovation programme under the Marie Skłodowska-Curie grant agreement No 860881-HIDDeN.

Appendix A: Model details

1. Loop-induced kinetic mixing in $U(1)_{L_i - L_j}$

In this section, we discuss the computation of the one-loop induced kinetic mixing. In this work we are mainly interested in $U(1)_{L_\mu - L_\tau}$, however, this discussion is generic for all $U(1)_{L_i - L_j}$ with $i, j = e, \mu, \tau$.

Since part of the SM leptons are charged under both the SM hypercharge $U(1)_Y$ and the new leptophilic gauge group $U(1)_{L_i - L_j}$, a kinetic mixing term between the new gauge boson and the hypercharge boson as well as the neutral $SU(2)_L$ boson is induced at the one-loop level [59],

$$\epsilon_B^{ij}(q^2) = \frac{g'\, g_{ij}}{8\pi^2} \int_0^1 dx\, x(1-x) \left[3 \log\left(\frac{m_i^2 - x(1-x)q^2}{m_j^2 - x(1-x)q^2} \right) + \log\left(\frac{m_{\nu_i}^2 - x(1-x)q^2}{m_{\nu_j}^2 - x(1-x)q^2} \right) \right] , \tag{A1}$$

$$\epsilon_W^{ij}(q^2) = \frac{g\, g_{ij}}{8\pi^2} \int_0^1 dx\, x(1-x) \left[\log\left(\frac{m_i^2 - x(1-x)q^2}{m_j^2 - x(1-x)q^2} \right) - \log\left(\frac{m_{\nu_i}^2 - x(1-x)q^2}{m_{\nu_j}^2 - x(1-x)q^2} \right) \right] . \tag{A2}$$

In the physical basis of neutral photon and Z boson, the mixings with the new leptophilic gauge boson read

$$\epsilon_A^{ij}(q^2) = \frac{e\, g_{ij}}{2\pi^2} \int_0^1 dx\, x(1-x)\ \log\left(\frac{m_i^2 - x(1-x)q^2}{m_j^2 - x(1-x)q^2} \right) , \tag{A3}$$

$$\epsilon_Z^{ij}(q^2) = -\frac{g_z\, g_{ij}}{4\pi^2} \int_0^1 dx\, x(1-x) \left[\log\left(\frac{m_i^2 - x(1-x)q^2}{m_j^2 - x(1-x)q^2} \right) + \log\left(\frac{m_{\nu_i}^2 - x(1-x)q^2}{m_{\nu_j}^2 - x(1-x)q^2} \right) \right] . \tag{A4}$$

Since the typical core temperature of a white dwarf is of the order of ~ 10 keV, it is safe to assume that the typical energy transfer q^2 at which the plasmon decay is happening, is much larger than the neutrino masses, $q^2 \gg m_\nu^2$. Thus, we can expand the second term in Eq. (A4),

$$\log\left(\frac{m_{\nu_i}^2/q^2 - x(1-x)}{m_{\nu_j}^2/q^2 - x(1-x)} \right) \approx \log\left(\frac{x(1-x)}{x(1-x)} \right) = 0 , \tag{A5}$$

where the first approximation is valid almost everywhere in the interval $x \in [0, 1]$.

At the same time, the masses of the charged leptons are much larger than the WD temperatures, $q^2 \ll m_\ell^2$. Hence, we can also expand the logarithms containing the charged lepton masses in Eqs. (A3) and (A4),

$$\log\left(\frac{m_i^2/m_j^2 - x(1-x)\ q^2/m_j^2}{1 - x(1-x)\ q^2/m_j^2} \right) \approx \log\left(\frac{m_i^2}{m_j^2} \right) , \tag{A6}$$

In summary, at typical WD temperatures, we can work with the q^2-independent approximations,

$$\epsilon_A^{ij} \approx \frac{e\, g_{ij}}{6\pi^2}\ \log\left(\frac{m_i}{m_j} \right) , \tag{A7}$$

$$\epsilon_Z^{ij} \approx -\frac{g_z\, g_{ij}}{12\pi^2}\ \log\left(\frac{m_i}{m_j} \right) = -\frac{1}{2} \frac{s_W}{c_W}\, \epsilon_A^{ij} . \tag{A8}$$

2. Interaction terms of the boson mass eigenstates

In order to obtain the interaction terms of the physical mass eigenstates of the neutral gauge bosons, we have to diagonalise both the kinetic and the mass terms in Eq. (1). Applying the full diagonalisation to the interaction terms, we obtain

$$\mathcal{L}_{\rm int} = -(A_\mu, Z_\mu, A'_\mu) \begin{pmatrix} e\, j^\mu_{\rm EM} \\ \frac{1}{\tau}\sqrt{\frac{\kappa-1}{2\,\kappa}}\left[g_x\, j^\mu_x - e\,\epsilon_A\, j^\mu_{\rm EM} - g_z\left(\epsilon_Z - \tau\sqrt{\frac{\kappa+1}{\kappa-1}}\right) j^\mu_Z\right] \\ \frac{1}{\tau}\sqrt{\frac{\kappa+1}{2\,\kappa}}\left[g_x\, j^\mu_x - e\,\epsilon_A\, j^\mu_{\rm EM} - g_z\left(\epsilon_Z + \tau\sqrt{\frac{\kappa-1}{\kappa+1}}\right) j^\mu_Z\right] \end{pmatrix}, \tag{A9}$$

with the definitions

$$\tau = \sqrt{1-\epsilon_A^2-\epsilon_Z^2}\,, \tag{A10}$$

$$\kappa = \sqrt{1+4\left(\frac{\epsilon_Z}{\delta-1}\right)^2}\,, \tag{A11}$$

$$\delta = \left(\frac{M_X}{M_Z}\right)^2. \tag{A12}$$

Since we are considering the mass range $M_X \ll M_Z$ we can approximate $\delta \approx 0$. Furthermore, we are mostly interested in the parameter space where $g_x < 10^{-2}$, such that $\epsilon_A \lesssim 10^{-4}$. To linear order in the the small parameters ϵ_A and ϵ_Z, we then get

$$\mathcal{L}_{\rm int} \approx -(A_\mu, Z_\mu, A'_\mu) \begin{pmatrix} e\, j^\mu_{\rm EM} \\ g_z\, j^\mu_Z \\ g_x\, j^\mu_x - e\,\epsilon_A\, j^\mu_{\rm EM} - g_z\,\epsilon_Z\, j^\mu_Z \end{pmatrix}. \tag{A13}$$

Hence, we recover the familiar SM photon and Z interactions with the electromagnetic and Z currents as defined in Eqs. (6) and (7), respectively. The mass eigenstate of the $U(1)_{L_\mu - L_\tau}$ gauge boson A', however, not only couples to the $U(1)_{L_\mu - L_\tau}$ current but picks up an additional interaction with the electromagnetic and Z current suppressed by the kinetic mixings ϵ_A and ϵ_Z, respectively.

[1] R. Foot, "New Physics From Electric Charge Quantization?," *Mod. Phys. Lett. A* **6** (1991) 527–530.

[2] X. G. He, G. C. Joshi, H. Lew, and R. R. Volkas, "NEW Z-prime PHENOMENOLOGY," *Phys. Rev. D* **43** (1991) 22–24.

[3] X.-G. He, G. C. Joshi, H. Lew, and R. R. Volkas, "Simplest Z-prime model," *Phys. Rev. D* **44** (1991) 2118–2132.

[4] R. Foot, X. G. He, H. Lew, and R. R. Volkas, "Model for a light Z-prime boson," *Phys. Rev. D* **50** (1994) 4571–4580, arXiv:hep-ph/9401250.

[5] J. Heeck and W. Rodejohann, "Gauged $L_\mu - L_\tau$ Symmetry at the Electroweak Scale," *Phys. Rev. D* **84** (2011) 075007, arXiv:1107.5238 [hep-ph].

[6] K. Asai, K. Hamaguchi, N. Nagata, S.-Y. Tseng, and K. Tsumura, "Minimal Gauged $\mathrm{U}(1)_{L_\alpha - L_\beta}$ Models Driven into a Corner," *Phys. Rev. D* **99** (2019) no. 5, 055029, arXiv:1811.07571 [hep-ph].

[7] M. Bauer, P. Foldenauer, and M. Mosny, "Flavor structure of anomaly-free hidden photon models," *Phys. Rev. D* **103** (2021) no. 7, 075024, arXiv:2011.12973 [hep-ph].

[8] C. Majumdar, S. Patra, P. Pritimita, S. Senapati, and U. A. Yajnik, "Neutrino mass, mixing and muon g − 2 explanation in $\mathrm{U}(1)_{L_\mu - L_\tau}$ extension of left-right theory," *JHEP* **09** (2020) 010, arXiv:2004.14259 [hep-ph].

[9] S. Baek and P. Ko, "Phenomenology of U(1)(L(mu)-L(tau)) charged dark matter at PAMELA and colliders," *JCAP* **10** (2009) 011, arXiv:0811.1646 [hep-ph].

[10] S. Baek, "Dark matter and muon $(g-2)$ in local $U(1)_{L_\mu - L_\tau}$-extended Ma Model," *Phys. Lett. B* **756** (2016) 1–5, arXiv:1510.02168 [hep-ph].

[11] A. Biswas, S. Choubey, and S. Khan, "Neutrino Mass, Dark Matter and Anomalous Magnetic Moment of Muon in a $U(1)_{L_\mu - L_\tau}$ Model," *JHEP* **09** (2016) 147, arXiv:1608.04194 [hep-ph].

[12] A. Biswas, S. Choubey, and S. Khan, "FIMP and Muon $(g-2)$ in a $\mathrm{U}(1)_{L_\mu - L_\tau}$ Model," *JHEP* **02** (2017) 123, arXiv:1612.03067 [hep-ph].

[13] P. Foldenauer, "Light dark matter in a gauged $U(1)_{L_\mu - L_\tau}$ model," *Phys. Rev. D* **99** (2019) no. 3, 035007, arXiv:1808.03647 [hep-ph].

[14] N. Okada and O. Seto, "Inelastic extra $U(1)$ charged scalar dark matter," *Phys. Rev. D* **101** (2020) no. 2, 023522, arXiv:1908.09277 [hep-ph].

[15] I. Holst, D. Hooper, and G. Krnjaic, "Simplest and Most Predictive Model of Muon g-2 and Thermal Dark Matter," *Phys. Rev. Lett.* **128** (2022) no. 14, 141802, arXiv:2107.09067 [hep-ph].
[16] S. Baek, N. G. Deshpande, X. G. He, and P. Ko, "Muon anomalous g-2 and gauged L(muon) - L(tau) models," *Phys. Rev. D* **64** (2001) 055006, arXiv:hep-ph/0104141.
[17] E. Ma, D. P. Roy, and S. Roy, "Gauged L(mu) - L(tau) with large muon anomalous magnetic moment and the bimaximal mixing of neutrinos," *Phys. Lett. B* **525** (2002) 101–106, arXiv:hep-ph/0110146.
[18] K. Harigaya, T. Igari, M. M. Nojiri, M. Takeuchi, and K. Tobe, "Muon g-2 and LHC phenomenology in the $L_\mu - L_\tau$ gauge symmetric model," *JHEP* **03** (2014) 105, arXiv:1311.0870 [hep-ph].
[19] W. Altmannshofer, C.-Y. Chen, P. S. Bhupal Dev, and A. Soni, "Lepton flavor violating Z' explanation of the muon anomalous magnetic moment," *Phys. Lett. B* **762** (2016) 389–398, arXiv:1607.06832 [hep-ph].
[20] M. Escudero, D. Hooper, G. Krnjaic, and M. Pierre, "Cosmology with A Very Light $L_\mu - L_\tau$ Gauge Boson," *JHEP* **03** (2019) 071, arXiv:1901.02010 [hep-ph].
[21] J. A. Carpio, K. Murase, I. M. Shoemaker, and Z. Tabrizi, "High-energy cosmic neutrinos as a probe of the vector mediator scenario in light of the muon g-2 anomaly and Hubble tension," *Phys. Rev. D* **107** (2023) no. 10, 103057, arXiv:2104.15136 [hep-ph].
[22] T. Araki, K. Asai, K. Honda, R. Kasuya, J. Sato, T. Shimomura, and M. J. S. Yang, "Resolving the Hubble tension in a $\mathrm{U}(1)_{L_\mu - L_\tau}$ model with the Majoron," *PTEP* **2021** (2021) no. 10, 103B05, arXiv:2103.07167 [hep-ph].
[23] W. Altmannshofer, S. Gori, M. Pospelov, and I. Yavin, "Quark flavor transitions in $L_\mu - L_\tau$ models," *Phys. Rev. D* **89** (2014) 095033, arXiv:1403.1269 [hep-ph].
[24] A. Crivellin, G. D'Ambrosio, and J. Heeck, "Explaining $h \to \mu^\pm\tau^\mp$, $B \to K^*\mu^+\mu^-$ and $B \to K\mu^+\mu^-/B \to Ke^+e^-$ in a two-Higgs-doublet model with gauged $L_\mu - L_\tau$," *Phys. Rev. Lett.* **114** (2015) 151801, arXiv:1501.00993 [hep-ph].
[25] W. Altmannshofer, S. Gori, S. Profumo, and F. S. Queiroz, "Explaining dark matter and B decay anomalies with an $L_\mu - L_\tau$ model," *JHEP* **12** (2016) 106, arXiv:1609.04026 [hep-ph].
[26] C.-H. Chen and T. Nomura, "Penguin $b \to s\ell'^+\ell'^-$ and B-meson anomalies in a gauged $L_\mu - L_\tau$," *Phys. Lett. B* **777** (2018) 420–427, arXiv:1707.03249 [hep-ph].
[27] S. Baek, "Dark matter contribution to $b \to s\mu^+\mu^-$ anomaly in local $U(1)_{L_\mu - L_\tau}$ model," *Phys. Lett. B* **781** (2018) 376–382, arXiv:1707.04573 [hep-ph].
[28] D. W. P. Amaral, D. G. Cerdeno, A. Cheek, and P. Foldenauer, "Confirming $U(1)_{L_\mu - L_\tau}$ as a solution for $(g-2)_\mu$ with neutrinos," *Eur. Phys. J. C* **81** (2021) no. 10, 861, arXiv:2104.03297 [hep-ph].
[29] Y. Kaneta and T. Shimomura, "On the possibility of a search for the $L_\mu - L_\tau$ gauge boson at Belle-II and neutrino beam experiments," *PTEP* **2017** (2017) no. 5, 053B04, arXiv:1701.00156 [hep-ph].
[30] D. W. P. d. Amaral, D. G. Cerdeno, P. Foldenauer, and E. Reid, "Solar neutrino probes of the muon anomalous magnetic moment in the gauged $\mathrm{U}(1)_{L_\mu - L_\tau}$," *JHEP* **12** (2020) 155, arXiv:2006.11225 [hep-ph].
[31] A. Kamada and H.-B. Yu, "Coherent Propagation of PeV Neutrinos and the Dip in the Neutrino Spectrum at IceCube," *Phys. Rev. D* **92** (2015) no. 11, 113004, arXiv:1504.00711 [hep-ph].
[32] A. Kamada, K. Kaneta, K. Yanagi, and H.-B. Yu, "Self-interacting dark matter and muon $g-2$ in a gauged $\mathrm{U}(1)_{L_\mu - L_\tau}$ model," *JHEP* **06** (2018) 117, arXiv:1805.00651 [hep-ph].
[33] D. Croon, G. Elor, R. K. Leane, and S. D. McDermott, "Supernova Muons: New Constraints on Z' Bosons, Axions and ALPs," *JHEP* **01** (2021) 107, arXiv:2006.13942 [hep-ph].
[34] D. G. Cerdeño, M. Cermeño, and Y. Farzan, "Constraints from the duration of supernova neutrino burst on on-shell light gauge boson production by neutrinos," *Phys. Rev. D* **107** (2023) no. 12, 123012, arXiv:2301.00661 [hep-ph].
[35] R. P. Feynman, N. Metropolis, and E. Teller, "Equations of State of Elements Based on the Generalized Fermi-Thomas Theory," *Phys. Rev.* **75** (1949) 1561–1573.
[36] E. E. Salpeter, "Energy and Pressure of a Zero-Temperature Plasma," *Astrophys. J.* **134** (1961) 669–682.
[37] M. Rotondo, J. A. Rueda, R. Ruffini, and S.-S. Xue, "The Relativistic Feynman-Metropolis-Teller theory for white dwarfs in general relativity," *Phys. Rev. D* **84** (2011) 084007, arXiv:1012.0154 [astro-ph.SR].
[38] A. Mathew and M. K. Nandy, "General relativistic calculations for white dwarfs," *Research in Astronomy and Astrophysics* **17** (2017) no. 6, 061.
[39] R. Fantoni, "White-dwarf equation of state and structure: the effect of temperature," *J. Stat. Mech.* **1711** (2017) no. 11, 113101, arXiv:1709.06064 [astro-ph.SR].
[40] D. E. Winget, D. J. Sullivan, T. S. Metcalfe, S. D. Kawaler, and M. H. Montgomery, "A strong test of electro-weak theory using pulsating db white dwarf stars as plasmon

neutrino detectors," *Astrophys. J. Lett.* **602** (2004) L109–L112, arXiv:astro-ph/0312303.

[41] E. M. Kantor and M. E. Gusakov, "The neutrino emission due to plasmon decay and neutrino luminosity of white dwarfs," *Mon. Not. Roy. Astron. Soc.* **381** (2007) 1702, arXiv:0708.2093 [astro-ph].

[42] J. D. Landstreet, "Synchrotron Radiation of Neutrinos and Its Astrophysical Significance," *Phys. Rev.* **153** (1967) 1372–1377.

[43] P. R. Chaudhuri, "Neutrino Synchrotron Radiation. I: Application to White Dwarfs," *Astrophysics and Space Science* **8** (1970) no. 3, 432–447.

[44] V. Canuto, C. Chiuderi, and C. K. Chou, "Plasmon neutrinos emission in a strong magnetic field. i: Transverse plasmons," *Astrophys. Space Sci.* **7** (1970) 407–415.

[45] V. Canuto, C. Chiuderi, and C. K. Chou, "Plasmon neutrinos emission in a strong magnetic field. ii: Longitudinal plasmons," *Astrophys. Space Sci.* **7** (1970) 453–460.

[46] D. Galtsov and N. Nikitina, "Photoneutrino processes in a strong field," *Sov. Phys. JETP* **35** (1972) 1047.

[47] L. L. DeRaad, Jr., K. A. Milton, and N. D. Hari Dass, "Photon Decay Into Neutrinos in a Strong Magnetic Field," *Phys. Rev. D* **14** (1976) 3326.

[48] V. Skobelev, "Reaction whereby a photon decays into a neutrino-antineutrino pair and a neutrino decays into a photon-neutrino pair in a strong magnetic field," *Zhurnal Eksperimentalnoi i Teoreticheskoi Fiziki* **71** (1976) 1263–1267.

[49] D. G. Yakovlev and R. Tschaepe, "Synchrotron neutrino-pair radiation in neutron stars," *Astronomische Nachrichten* **302** (1981) no. 4, 167–176.

[50] A. D. Kaminker, K. P. Levenfish, D. G. Yakovlev, P. Amsterdamski, and P. Haensel, "Neutrino emissivity from e- synchrotron and e-e+ annihilation processes in a strong magnetic field: General formalism and nonrelativistic limit," *Phys. Rev. D* **46** (1992) 3256–3264.

[51] M. P. Kennett and D. B. Melrose, "Neutrino emission via the plasma process in a magnetized plasma," *Phys. Rev. D* **58** (1998) 093011, arXiv:astro-ph/9901156.

[52] I. Bhattacharyya, "Neutrino synchrotron radiation in electro-weak interaction," *Astropart. Phys.* **24** (2005) 100–106.

[53] M. Drewes, J. McDonald, L. Sablon, and E. Vitagliano, "Neutrino Emissivities as a Probe of the Internal Magnetic Fields of White Dwarfs," *Astrophys. J.* **934** (2022) 99, arXiv:2109.06158 [astro-ph.SR].

[54] M. Bauer, P. Foldenauer, and J. Jaeckel, "Hunting All the Hidden Photons," *JHEP* **07** (2018) 094, arXiv:1803.05466 [hep-ph].

[55] H. K. Dreiner, J.-F. Fortin, J. Isern, and L. Ubaldi, "White Dwarfs constrain Dark Forces," *Phys. Rev. D* **88** (2013) 043517, arXiv:1303.7232 [hep-ph].

[56] **Planck** Collaboration, N. Aghanim *et al.*, "Planck 2018 results. VI. Cosmological parameters," *Astron. Astrophys.* **641** (2020) A6, arXiv:1807.06209 [astro-ph.CO]. [Erratum: Astron.Astrophys. 652, C4 (2021)].

[57] A. G. Riess, S. Casertano, W. Yuan, L. M. Macri, and D. Scolnic, "Large Magellanic Cloud Cepheid Standards Provide a 1% Foundation for the Determination of the Hubble Constant and Stronger Evidence for Physics beyond ΛCDM," *Astrophys. J.* **876** (2019) no. 1, 85, arXiv:1903.07603 [astro-ph.CO].

[58] N. Blinov, K. J. Kelly, G. Z. Krnjaic, and S. D. McDermott, "Constraining the Self-Interacting Neutrino Interpretation of the Hubble Tension," *Phys. Rev. Lett.* **123** (2019) no. 19, 191102, arXiv:1905.02727 [astro-ph.CO].

[59] M. Bauer and P. Foldenauer, "Consistent Theory of Kinetic Mixing and the Higgs Low-Energy Theorem," *Phys. Rev. Lett.* **129** (2022) no. 17, 171801, arXiv:2207.00023 [hep-ph].

[60] K. R. Lynch, "A Note on one loop electroweak contributions to g-2: A Companion to BUHEP-01-16," arXiv:hep-ph/0108081.

[61] M. Pospelov, "Secluded U(1) below the weak scale," *Phys. Rev. D* **80** (2009) 095002, arXiv:0811.1030 [hep-ph].

[62] T. Aoyama *et al.*, "The anomalous magnetic moment of the muon in the Standard Model," *Phys. Rept.* **887** (2020) 1–166, arXiv:2006.04822 [hep-ph].

[63] **Muon g-2** Collaboration, D. P. Aguillard *et al.*, "Measurement of the Positive Muon Anomalous Magnetic Moment to 0.20 ppm," *Phys. Rev. Lett.* **131** (2023) no. 16, 161802, arXiv:2308.06230 [hep-ex].

[64] **Muon g-2** Collaboration, B. Abi *et al.*, "Measurement of the Positive Muon Anomalous Magnetic Moment to 0.46 ppm," *Phys. Rev. Lett.* **126** (2021) no. 14, 141801, arXiv:2104.03281 [hep-ex].

[65] **Muon g-2** Collaboration, G. W. Bennett *et al.*, "Final Report of the Muon E821 Anomalous Magnetic Moment Measurement at BNL," *Phys. Rev. D* **73** (2006) 072003, arXiv:hep-ex/0602035.

[66] S. Borsanyi *et al.*, "Leading hadronic contribution to the muon magnetic moment from lattice QCD," *Nature* **593** (2021) no. 7857, 51–55, arXiv:2002.12347 [hep-lat].

[67] A. Crivellin, M. Hoferichter, C. A. Manzari, and M. Montull, "Hadronic Vacuum Polarization: $(g-2)_\mu$ versus Global Electroweak Fits," *Phys. Rev. Lett.* **125** (2020) no. 9, 091801, arXiv:2003.04886 [hep-ph].

[68] J. H. Zink and M. E. Ramirez-Quezada, "Exploring the dark sectors via the cooling of

white dwarfs," *Phys. Rev. D* **108** (2023) no. 4, 043014, arXiv:2306.00517 [hep-ph].

[69] E. Braaten and D. Segel, "Neutrino energy loss from the plasma process at all temperatures and densities," *Phys. Rev. D* **48** (1993) 1478–1491, arXiv:hep-ph/9302213.

[70] S. L. Shapiro and S. A. Teukolsky, "Black holes, white dwarfs and neutron stars. The physics of compact objects," *Wiley, New York* **19832** (1983) 119–123.

[71] G. Breit and E. Wigner, "Capture of Slow Neutrons," *Phys. Rev.* **49** (1936) 519–531.

[72] H. A. Weldon, "Simple Rules for Discontinuities in Finite Temperature Field Theory," *Phys. Rev. D* **28** (1983) 2007.

[73] G. P. Lepage, "Adaptive multidimensional integration: VEGAS enhanced," *J. Comput. Phys.* **439** (2021) 110386, arXiv:2009.05112 [physics.comp-ph].

[74] B. M. S. Hansen, H. Richer, J. Kalirai, R. Goldsbury, S. Frewen, and J. Heyl, "Constraining Neutrino Cooling using the Hot White Dwarf Luminosity Function in the Globular Cluster 47 Tucanae," *Astrophys. J.* **809** (2015) no. 2, 141, arXiv:1507.05665 [astro-ph.SR].

[75] Y. M. Andreev *et al.*, "Exploration of the Muon $g-2$ and Light Dark Matter explanations in NA64 with the CERN SPS high energy muon beam," arXiv:2401.01708 [hep-ex].

[76] G. Bellini *et al.*, "Precision measurement of the 7Be solar neutrino interaction rate in Borexino," *Phys. Rev. Lett.* **107** (2011) 141302, arXiv:1104.1816 [hep-ex].

[77] **Borexino** Collaboration, M. Agostini *et al.*, "First Simultaneous Precision Spectroscopy of *pp*, ^{7}Be, and *pep* Solar Neutrinos with Borexino Phase-II," *Phys. Rev. D* **100** (2019) no. 8, 082004, arXiv:1707.09279 [hep-ex].

[78] **BaBar** Collaboration, J. P. Lees *et al.*, "Search for a muonic dark force at BABAR," *Phys. Rev. D* **94** (2016) no. 1, 011102, arXiv:1606.03501 [hep-ex].

[79] **COHERENT** Collaboration, D. Akimov *et al.*, "The COHERENT Experiment at the Spallation Neutron Source," arXiv:1509.08702 [physics.ins-det].

[80] **COHERENT** Collaboration, D. Akimov *et al.*, "Observation of Coherent Elastic Neutrino-Nucleus Scattering," *Science* **357** (2017) no. 6356, 1123–1126, arXiv:1708.01294 [nucl-ex].

[81] W. Altmannshofer, S. Gori, M. Pospelov, and I. Yavin, "Neutrino Trident Production: A Powerful Probe of New Physics with Neutrino Beams," *Phys. Rev. Lett.* **113** (2014) 091801, arXiv:1406.2332 [hep-ph].

[82] **CHARM-II** Collaboration, D. Geiregat *et al.*, "First observation of neutrino trident production," *Phys. Lett. B* **245** (1990) 271–275.

[83] G. Krnjaic, G. Marques-Tavares, D. Redigolo, and K. Tobioka, "Probing Muonphilic Force Carriers and Dark Matter at Kaon Factories," *Phys. Rev. Lett.* **124** (2020) no. 4, 041802, arXiv:1902.07715 [hep-ph].

[84] P. Lepage, "gplepage/vegas: vegas version 6.0." Zenodo, Mar., 2024. https://doi.org/10.5281/zenodo.10783443.